

A framework for computing effective boundary conditions at the interface between free fluid and a porous medium

Uģis Lācis and Shervin Bagheri[†]

Linné Flow Centre, Department of Mechanics KTH, SE-100 44 Stockholm, Sweden

(Received 9 December 2024)

Interfacial boundary conditions determined from empirical or *ad-hoc* models remain the standard approach to model fluid flows over porous media, even in situations where the topology of the porous medium is known. We propose a non-empirical and accurate method to compute the effective boundary conditions at the interface between a porous surface and an overlying flow. Using multiscale expansion (homogenization) approach, we derive a tensorial generalized version of the empirical condition suggested by Beavers & Joseph (1967). The components of the tensors determining the effective slip velocity at the interface are obtained by solving a set of Stokes equations in a small computational domain near the interface containing both free flow and porous medium. Using the lid-driven cavity flow with a porous bed, we demonstrate that the derived boundary condition is accurate and robust by comparing an effective model to direct numerical simulations. Finally, we provide an open source code that solves the microscale problems and computes the velocity boundary condition without free parameters over any porous bed.

1. Introduction

Surfaces found in nature are generally non-smooth with complex hierarchical structural features (Liu & Jiang 2011). The purpose of these surfaces vary greatly, ranging from camouflage and insulation to less obvious functions, such as passively interacting with surrounding fluid to reduce drag or noise (Abdulbari *et al.* 2013). These functions manifest as effective macroscale properties – for example, permeability, elasticity, slip and optical transparency – while the origin is the small-scale features of the surface. Therefore, to understand the hydrodynamic function of such complex surfaces, a systematic multi-scale approach is required. In a bottom-up strategy, the microscale fluid-structure physics of the coating material is analyzed first; the effective porosity, elasticity or slip are then induced naturally by upscaling the microscale features.

Volume-averaging and homogenization techniques (Davit *et al.* 2013) enable a bottom-up strategy by deriving the effective equations governing the macroscale coating dynamics, which contains parameters arising from microscale features. Whereas these techniques are routinely applied for homogeneous materials (e.g. the interior of a material), their application to inhomogeneous regions (e.g. near interfaces) has not reached the same level of maturity. One example, which is also the focus of the present work, is the interface between an overlying flow and a rigid porous surface. Recent work (Ochoa-Tapia & Whitaker 1995; Mikelić & Jäger 2000; Auriault 2010; Minale 2014) have treated the inhomogeneous interface problem theoretically with upscaling techniques. Ochoa-Tapia

[†] Email address for correspondence: shervin@mech.kth.se

& Whitaker (1995) used a volume-averaging technique to derive a shear-stress jump condition. Recently, Minale (2014) re-derived the boundary conditions of Ochoa-Tapia & Whitaker (1995), elucidating how the stress from the free fluid is partitioned between the porous skeleton and the porous flow.

Volume-averaging techniques induce closure problems that need to be resolved using scale estimates. A homogenization technique, on the other hand, begins with scale estimates and an expansion in small parameter $\epsilon = l/L$, defining the scale separation between microscale l and macroscale L ; it results in equations at different orders of ϵ and a decoupling of different quantities and thus also in simpler closure problems. Mikelić & Jäger (2000) used homogenization and method of matched asymptotic expansions to show that the Saffman (1971) version of the empirical boundary condition by Beavers & Joseph (1967) (called BJ condition hereafter) is mathematically justified and its slip parameter can be computed by solving microscale problems in an interface unit cell. Auriault (2010) also used a homogenization technique to derive a BJ-type of boundary condition valid for pressure-driven flows; he obtained however the condition at different order compared to Mikelić & Jäger (2000).

The boundary conditions derived using upscaling techniques have remained at a proof-of-concept level and only demonstrated on canonical one-dimensional flows. The theoretical progress has not yet resulted in a method that can in a straight-forward manner be applied by practitioners and engineers. The reason is to some extent the non-trivial mathematical aspects – such as closure problems. Another reason is that the focus has been on mathematically justifying empirical boundary conditions, rather than presenting a step-by-step method for computing interfacial conditions. Therefore, investigations of practical interest of flows over porous media continue using empirical conditions or conditions with free unknown parameters (Han *et al.* 2005; Le Bars & Worster 2006; Rosti *et al.* 2015; Zampogna & Bottaro 2016). Although these conditions provide physical models of the flow over porous media, they are based on lumping all unknown effects into few scalar parameters. This approach requires the support of empirical data (Zampogna & Bottaro 2016) or extensive computations to cover a large interval of parameters (Rosti *et al.* 2015).

In this work, we provide practitioners the framework to compute accurate interfacial velocity boundary conditions, instead of empirically determining them. We derive the interface boundary condition for slip velocity using homogenization and present the relevant Stokes equations to be solved in a microscale interface unit cell. Our main contribution is to provide a set of simple and numerically feasible microscale problems without closure models, which once solved, allows for a robust non-empirical effective interface condition. Our interface equation can be considered as a generalized version of the BJ condition, since it depends on interface tensors and on the total fluid stress.

2. Direct numerical simulations versus continuum model

The method that we propose is general, but will for simplicity be exemplified on the lid-driven cavity flow with a homogenous bed of solid cylinders of diameter $D = 2r$ as shown schematically in Fig. 1a. The cavity has a length L and a depth of $(H + d)$, where the porous bed is confined to $-d < y < 0$ and $-L/2 < x < L/2$. The top wall of the cavity is driven by a constant streamwise velocity U_w . The two-dimensional Stokes equations are solved with no-slip conditions imposed at the cylinder surfaces as well as on the vertical and bottom walls of the cavity. Fig. 2a,b (solid black) shows the streamwise and wall-normal velocity profiles for the streamwise position $x/L = -0.1$, solid volume fraction $\phi = \pi r^2/l^2 = 0.02$ and pore scale $l/H = 0.1$. The computations

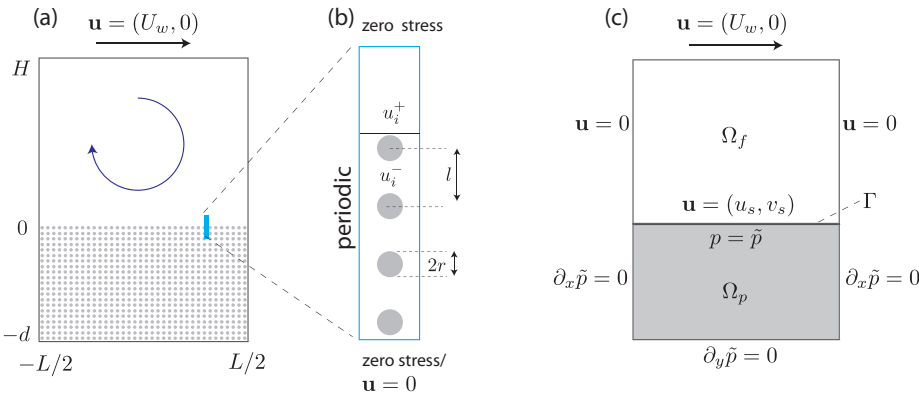


FIGURE 1. Left frame (a) shows the lid-driven cavity flow with a porous bed, where the flow is obtained using full DNS. Center frame (b) shows the interface unit cell used for solving microscale problems in order to determine coefficients of the effective boundary condition. Right frame (c) shows the continuum two-domain approach of the porous cavity.

are performed with FreeFEM++ (Hecht 2012), using a triangular mesh and a Taylor-Hood finite element space (P2+P1) for velocity and pressure. We use mesh spacing of $\Delta s = 0.033l$ at the outer part of the domain, and $\Delta s = 0.020l$ at the surface of cylinders.

The insets in Fig. 2 show microscale fluctuations of the velocities in the interior domain of the porous bed (in particular for v -component), and then a rapid transition to the macroscale velocity in the free fluid region. This transition occurs in a thin layer near the top row of cylinders. If this layer is substituted with an interface placed at $y_s/l = 0.1$, we observe that the velocity at this interface will have a streamwise slip velocity of $u_s/U_w = -0.0085$. In the same figures, results of the cavity flow with a no-slip condition at $y_s/l = 0.1$ are shown (red line), where a clear deviation of the profile over the porous domain is observed. The choice of interface location y_s is arbitrary; we will show in the final section of this paper that our boundary condition is essentially independent of this location. Although the slip velocities are small compared to the bulk flow, they may have a significant physical effect on the characteristics of the overlying fluid. For example Rosti *et al.* (2015) showed recently that slip velocities below 3% had a significant effect on the flow statistics in a turbulent channel.

Fig. 2a,b (blue curve with diamond symbols) show the velocity profiles obtained with a computationally cheaper two-domain approach based on modeling the porous medium with a continuum model (Fig. 1c). As derived for example by Mei & Vernescu (2010), the governing equations for the fluid flow and pore pressure are

$$\begin{aligned} -\nabla p + \mu \Delta \mathbf{u} &= 0 && \text{in } \Omega_f, \\ \nabla \cdot \mathbf{u} &= 0 && \text{in } \Omega_f, \\ \Delta \tilde{p} &= 0 && \text{in } \Omega_p, \end{aligned}$$

where μ is the fluid viscosity, and Ω_f and Ω_p denote the free fluid and porous domains, respectively. Dirichlet conditions are imposed for the free fluid (\mathbf{u}) on the the vertical side walls and the top wall of the cavity (as for the full DNS), whereas for the pore pressure (\tilde{p}) Neumann conditions are imposed on the side walls and the bottom wall. The boundary conditions at the interface Γ between the two domains are

$$\mathbf{u} = (u_s, v_s), \quad \tilde{p} = p, \quad \text{at } \Gamma.$$

Here, to solve for pressure field in the porous region, we have imposed pressure continuity

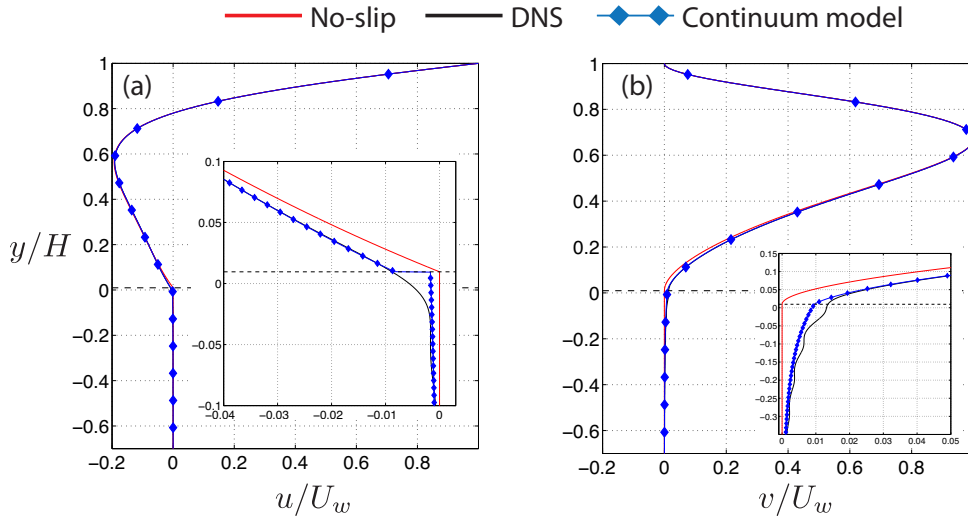


FIGURE 2. In (a) and (b), solid black and red lines depict direct numerical simulations of the porous cavity problem and a no-slip cavity problem, respectively. Blue lines correspond to the continuum model of the porous bed coupled to Stokes solver above the bed via interface conditions at $y_s/H = 0.01$, which is equivalent to $y_s/l = 0.1$ in pore scale.

at the interface, which is valid for this particular microstructure. From mass conservation it follows that the normal velocity component v_s equals the interior seepage velocity,

$$v_s = -\frac{K_{cyl}}{\mu} \partial_y \tilde{p}, \quad (2.1)$$

where K_{cyl} is the isotropic permeability of the porous medium consisting of a regular array of circular cylinders. The condition for streamwise velocity u_s is

$$u_s = -\frac{K_s}{\mu} \partial_x p + L_s (\partial_y u + \partial_x v), \quad (2.2)$$

which is similar to the condition obtained empirically by Beavers and Joseph, except that K_s is the interface permeability $K_s \neq K_{cyl}$, related to a semi-permeable transition layer between the porous medium and the free fluid. Another difference with the BJ condition is that the strain term $\partial_x v$ is included in addition to $\partial_y u$. It has been argued that the term $\partial_x v$ should be present for curved boundaries (Jones 1973), but to the authors' knowledge, it has not been derived earlier for flat interfaces (Nield 2009). The constant L_s is related to the slip length in the Navier boundary condition.

In Fig. 2, we observe a good agreement between DNS and the continuum model, despite that the latter does not resolve the microscale dynamics between and around the cylinders. The model is able to predict the streamwise slip velocity at the interface, $u_s/U_w = -0.0082$. Therefore, from the perspective of the free fluid, the effect of the porous bed is essentially the same using fully resolved DNS and the continuum model, as can be seen by the nearly perfect match between the profiles in the free fluid region.

3. Interface problem and effective boundary conditions

We now turn our attention to the small interface unit cell depicted in Fig. 1b. Using this domain, the flow in the transition layer will be characterized and used to find interface conditions for larger and more complex domains, such as the cavity. We define a scale-

separation parameter as $\epsilon = l/L \ll 1$, where $L \sim H$. When the inertial effects in the porous medium are small, the local microscopic viscous force is balanced by the macroscopic pressure force,

$$\frac{\Delta P}{L} \sim \frac{\mu U^d}{l^2}.$$

Here, ΔP is the characteristic pressure difference and U^d is the characteristic velocity in the porous region. We write the Navier-Stokes equations in dimensionless form

$$\epsilon^2 Re_d (\partial_t u_i + u_j u_{i,j}) = -p_{,i} + \epsilon u_{i,jj}, \quad (3.1)$$

$$u_{i,i} = 0, \quad (3.2)$$

where $Re_d = U^d L / \nu$ is the Darcy Reynolds number.

We start by choosing an interface at a vertical coordinate $x_2 = y_s$, which divides the interface cell into a free fluid region and a porous region. The final interface condition does not depend on y_s (up to certain limits) as we will discuss later. We separate the flow above the interface ($y \geq y_s$) into a fast flow (U_i, P) and a perturbation (u_i^+, p^+),

$$u_i = U_i + u_i^+, \quad p = P + p^+, \quad (3.3)$$

where $\|u_i^+\| \ll \|U_i\|$ and $\|p_i^+\| \ll \|P\|$. We then insert the decomposition (3.3) into equations (3.1–3.2) and group the different terms. The fast flow U_i is governed by the Navier-Stokes equations with no-slip condition at y_s . The perturbation terms (u_i^+, p^+) will – as shown below – be responsible for the induced slip in the effective boundary conditions; they are described by

$$\mathcal{A}(u_i^+, p^+, \epsilon) = \epsilon^2 Re_d (\partial_t u_i^+ + u_j^+ u_{i,j}^+ + U_j u_{i,j}^+ + u_j^+ U_{i,j}). \quad (3.4)$$

We have defined a linear Stokes operator $\mathcal{A}(u_i, p, \epsilon) = R_i : -p_{,i} + \epsilon u_{i,jj} = R_i, u_{i,i} = 0, u_i|_{\Gamma_C} = 0$ where Γ_C is the solid boundary of cylinders and R_i is a right-hand term, usually containing the inertial terms. Below the interface and in the porous bed ($y \leq y_s$), the pressure and the slow velocity, denoted by $\tilde{u}_i = u_i^-$ and $\tilde{p} = p^-$, are governed by

$$\mathcal{A}(u_i^-, p^-, \epsilon) = \epsilon^2 Re_d (\partial_t u_i^- + u_j^- u_{i,j}^-). \quad (3.5)$$

Next, we introduce a macroscale coordinate $X_i \sim L$ and a microscale coordinate $x_i \sim l$, which are appropriate to describe the macroscopic and microscopic variations, respectively. We then carry out a multi-scale expansion

$$u_i^\pm(X_i, x_i) = u_i^{\pm(0)}(X_i, x_i) + \epsilon u_i^{\pm(1)}(X_i, x_i) + \epsilon^2 u_i^{\pm(2)}(X_i, x_i) + \dots$$

(similarly for p^\pm) and insert these expansions into the corresponding equations (3.4–3.5) above. The zeroth-order $\mathcal{O}(\epsilon^0)$ equations result in leading-order pressure terms $p^{\pm(0)}$ that are independent of the microscale coordinate x_i (Mei & Vernescu 2010). Collecting the first order terms $\mathcal{O}(\epsilon^1)$ results in two Stokes equations,

$$\mathcal{A}(u_i^{-(0)}, p^{-(1)}, 1) = \frac{1}{\epsilon} p_{,i}^{-(0)}(X_i) \quad (3.6)$$

and

$$\mathcal{A}(u_i^{+(0)}, p^{+(1)}, 1) = \frac{1}{\epsilon} p_{,i}^{+(0)}(X_i) = 0. \quad (3.7)$$

Here, $p_{,i}^{-(0)}(X_i)$ represents the pressure gradient that drives the flow through the porous bed. Above the interface the driving pressure is contained in P inducing the fast flow U_i ;

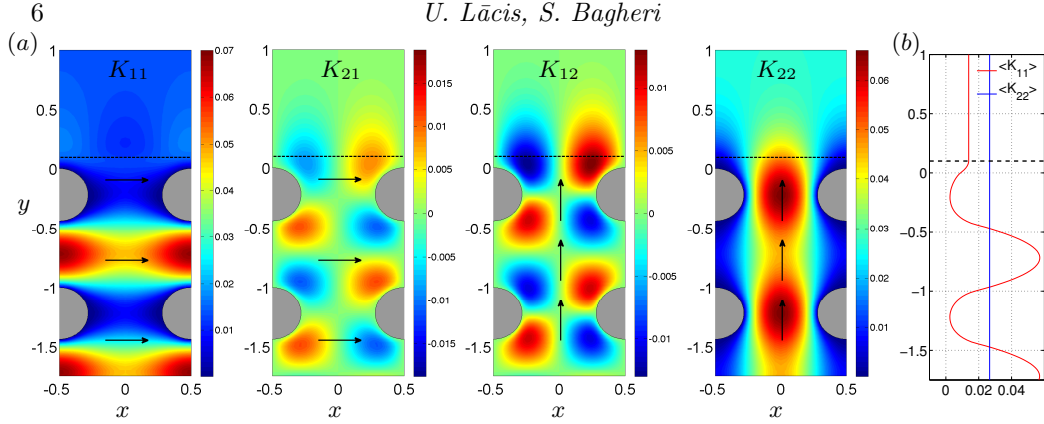


FIGURE 3. Solutions of interface problems for the coefficients of the Darcy term ($\phi = 0.15$ and $y_s = 0.1$). The frames from left to right correspond to the flow fields K_{11} , K_{21} , K_{12} and K_{22} . The arrows indicate the direction of the constant unit volume forcing below the interface (horizontal dashed line). Rightmost frame (b) shows plane-averaged profiles; the streamwise component provides the interface permeability ($\langle K_{11} \rangle = 0.014$ at y_s), whereas the wall-normal component is constant and corresponds to the interior permeability ($\langle K_{22} \rangle = 0.0266$).

therefore $p^{+(0)}(X_i) \approx p^+ = p - P$, represents the macroscale-varying pressure perturbation above the interface. We assume that this term is zero, since pressure fluctuations above the interface due to the porous bed can only vary at microscopic length scale.

The boundary conditions imposed at the interface y_s are continuity of velocity

$$u_i^{-(0)} = u_i^{+(0)} \quad (3.8)$$

and continuity of total stress

$$\Sigma_{ij}^{u^-(1)} n_j = \Sigma_{ij}^{u^+(1)} n_j + \frac{1}{\epsilon} \Sigma_{ij}^U n_j, \quad (3.9)$$

where $\Sigma_{ij}^{u^\pm(1)} = -p^{\pm(1)} \delta_{ij} + (u_{i,j}^{\pm(0)} + u_{j,i}^{\pm(0)})$ and $\Sigma_{ij}^U = -P \delta_{ij} + \epsilon (U_{i,j} + U_{j,i})$ are the fluid perturbation and no-slip fluid stress tensors, respectively. In contrast to previous work, the stress induced by the flow below the interface is balanced by the stress induced by the total flow $u_i \approx U_i + u_i^{+(0)}$ above the interface.

We may consider the Stokes equations (3.6–3.7) and the boundary conditions (3.8–3.9) as one linear problem with four unknowns $(u_i^{\pm(0)}, p^{\pm(1)})$. Due to linearity, we can construct the solutions for the velocity and pressure fields as superposition of $p_{,i}^{-(0)}(X_i)$ and $\Sigma_{ij}^U(X_i)$ (assuming that the interface stress is only a function of X_i), i.e.

$$u_i^{\pm(0)} = -K_{ij}^{\pm} \frac{1}{\epsilon} p_{,j}^{-(0)} + L_{ijk}^{\pm} \frac{1}{\epsilon} \Sigma_{jk}^U|_{y_s}, \quad (3.10)$$

and

$$p^{\pm(1)} = -A_j^{\pm} \frac{1}{\epsilon} p_{,j}^{-(0)} + B_{ij}^{\pm} \frac{1}{\epsilon} \Sigma_{ij}^U|_{y_s}. \quad (3.11)$$

The average of K_{ij} is a tensorial effective permeability and the average of L_{ijk} is related to the tensorial version of the Navier slip coefficient. Similarly, the tensors A_j and B_{ij} are transfer coefficients from the driving pressure gradient and fluid stress, respectively, to the perturbation pressure.

3.1. Microscale Stokes problems for Darcy term

By inserting the ansatzes (3.10-3.11) into equations (3.7–3.8), it follows that the tensors K_{ij}^\pm and A_i^\pm satisfy,

$$\begin{aligned}\mathcal{A}(K_{ik}^+, A_k^+, 1) &= 0 & y \geq y_s, \\ \mathcal{A}(K_{ik}^-, A_k^-, 1) &= -\delta_{ik} & y \leq y_s,\end{aligned}$$

with boundary conditions at the interface y_s given by

$$K_{ik}^- = K_{ik}^+, \quad \Sigma_{ij}^{K^+} n_j = \Sigma_{ij}^{K^-} n_j.$$

The component K_{jk}^\pm represents the j th velocity component of the k th Stokes problem. Thus to determine every component of K_{ij}^\pm and A_i^\pm , 3 pairs of Stokes problems have to be solved coupled at the interface through continuity of velocity field and stress. Note that below the interface, the flow is driven by a unit forcing in one direction at a time. Therefore the physical interpretation of K_{i1} , for example, is the flow response to forcing in the horizontal direction below the interface (see Fig. 3a).

To complete the formulation, we impose zero stress at the top and the bottom of the cell and periodic conditions at the vertical boundaries (see Fig. 1b). The interface cell needs to extend sufficiently into the free fluid such that variations of u^+ are small and sufficiently into the porous medium such that variations of u^- are periodic. Fig. 3 shows K_{ij} fields and corresponding plane averaged profiles for interface location $y_s = 0.1$.

3.2. Microscale Stokes problems for Navier-slip term

By inserting the ansatzes (3.10–3.11) into (3.7–3.8), the following equations for the tensors L_{ijk}^\pm and B_{ij}^\pm are obtained,

$$\begin{aligned}\mathcal{A}(L_{ikl}^+, B_{kl}^+, 1) &= 0 & y \geq y_s, \\ \mathcal{A}(L_{ikl}^-, B_{kl}^-, 1) &= 0 & y \leq y_s,\end{aligned}$$

with boundary conditions at y_s given by,

$$L_{ikl}^- = L_{ikl}^+, \quad \Sigma_{ij}^{L^+} n_j = \Sigma_{ij}^{L^-} n_j - \delta_{ik} n_l.$$

The tensors transferring the stress of the free fluid to the perturbation velocity require the solution of 9 pairs of coupled Stokes problem. The forcing for these equations is at the interface in the form of a stress condition. For example, the L_{i12} component is the flow response to a tangential stress at the interface, whereas the L_{i22} is the response to unit normal stress at the interface. In general, for problems with flat interfaces described in a coordinate system aligned with the interface, only three pairs of problems are forced.

Returning to our 2D configuration with a flat interface and aligned coordinate system, these microscale problems are solved with zero stress condition at the top, no-slip condition at the bottom of the cell and periodic boundary conditions on the vertical boundaries (Fig. 1b). The no-slip condition is chosen, because the contribution to porous flow driven by free-fluid stress dissipates rapidly inside the medium. In general however, the boundary conditions of the interface unit cell is a modelling process, which does not arise from the theory of multi-scale expansion. In our case, L_{ij1} are unforced problems, leading to trivial solution for all components. Out of the forced problems L_{ij2} , the components L_{122} and L_{222} are zero since the forcing is in a constrained direction, i.e. due to mass conservation the motion in vertical direction is zero when the no-slip condition is enforced at the bottom boundary. We are thus left with only one non-trivial problem

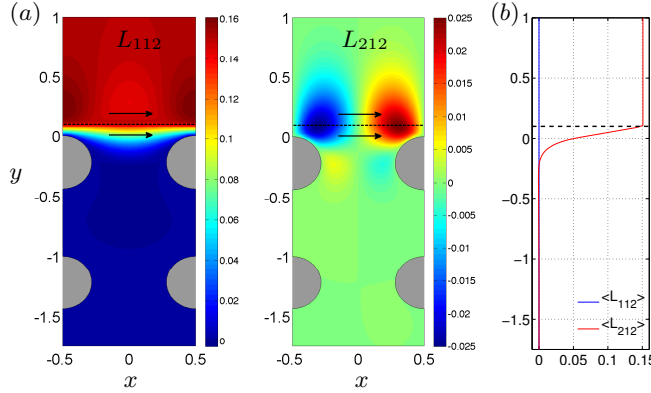


FIGURE 4. Solutions of interface problem for the non-zero component (L_{i12}) of the Navier-slip term ($\phi = 0.15$ and $y_s = 0.1$). The left and center frames correspond to L_{112} and L_{212} , respectively. The arrows indicate the direction of the constant unit boundary forcing at the interface location. Rightmost frame (b) shows plane-averaged profiles; the streamwise component provides the interface slip length ($\langle L_{112} \rangle = 0.15$ at y_s), whereas the average of wall-normal component is zero (i.e. $\langle L_{212} \rangle = 0$), since the 2D field is antisymmetric with respect to center axis.

(L_{i12}), for which the flows fields are shown in Fig. 4, along with corresponding plane averaged profiles.

3.3. Effective interface condition

We may now construct an effective boundary condition by taking the plane average $\langle \cdot \rangle$ of $u_i^{-(0)}$ (3.10) at the interface location,

$$\langle u_i^- \rangle \approx \langle u_i^{-(0)} \rangle = -\langle K_{ij}^- \rangle \frac{1}{\epsilon} p_{,j}^{-(0)} + \langle L_{ijk}^- \rangle \frac{1}{\epsilon} \Sigma_{jk}^U \quad \text{at} \quad \Gamma.$$

To arrive with the final form of the effective boundary condition, we assume that the microscale-varying perturbation stress is very small compared to the stress from the fast channel flow, i.e. $\Sigma_{ij}^{u+} \Big|_{y_s} \ll \Sigma_{ij}^U \Big|_{y_s}$, which means that $\Sigma_{ij}^U \Big|_{y_s} \approx \Sigma_{ij}^u \Big|_{y_s}$. In our numerical tests, we have observed that this assumption is exact for $y_s > 0$. Moreover, experiments by Beavers & Joseph (1967) also show that the leading order effect of the porous medium is a slip velocity, and not a modification of the velocity gradient near the wall.

Recalling that at interface $u_i = U_i + u_i^+ = u_i^{-(0)} + \mathcal{O}(\epsilon)$ and $\tilde{p} = p^{-(0)} + \mathcal{O}(\epsilon)$, we obtain

$$u_i = -\mathcal{K}_{ij} \frac{1}{\epsilon} \tilde{p}_{,j} + \mathcal{L}_{ijk} \frac{1}{\epsilon} \Sigma_{jk}^u \quad \text{at} \quad \Gamma,$$

where $\mathcal{K}_{ij} = \langle K_{ij}^- \rangle$ and $\mathcal{L}_{ijk} = \langle L_{ijk}^- \rangle$. This is the final expression for the velocity boundary condition for a rigid porous bed. It can be used together with Navier-Stokes equations (3.1–3.2) in any domain of interest, in order take into account the effects of the porous medium, without resolving the microscale flow within the bed. We emphasize that the “tilde” notation for pressure means that the pressure in the boundary condition is the pore pressure. The plane-average brackets from the velocity are removed, since the plane-averaged interface velocity is used as a point-wise boundary condition for the free fluid.

In order to return to the boundary conditions (2.1–2.2) used for the lid-driven cavity

y_s	ϵ	ϕ	u_K^{mod}	u_L^{mod}	u^{mod}	u^{DNS}
0.10	0.02	0.02	$3.16 \cdot 10^{-1}$	$4.52 \cdot 10^1$	$4.55 \cdot 10^1$	$4.56 \cdot 10^1$
		0.15	$5.03 \cdot 10^{-1}$	$1.42 \cdot 10^2$	$1.42 \cdot 10^2$	$1.42 \cdot 10^2$
		0.45	$3.95 \cdot 10^0$	$1.21 \cdot 10^3$	$1.21 \cdot 10^3$	$1.21 \cdot 10^3$
	0.10	0.02	$3.15 \cdot 10^{-1}$	$9.14 \cdot 10^0$	$9.46 \cdot 10^0$	$9.48 \cdot 10^0$
		0.15	$5.03 \cdot 10^{-1}$	$2.84 \cdot 10^1$	$2.89 \cdot 10^1$	$2.89 \cdot 10^1$
		0.45	$3.96 \cdot 10^0$	$2.40 \cdot 10^2$	$2.44 \cdot 10^2$	$2.44 \cdot 10^2$
0.50	0.02	0.02	$1.85 \cdot 10^0$	$1.44 \cdot 10^2$	$1.46 \cdot 10^2$	$1.46 \cdot 10^2$
		0.15	$5.67 \cdot 10^0$	$4.96 \cdot 10^2$	$5.02 \cdot 10^2$	$5.02 \cdot 10^2$
		0.45	$4.98 \cdot 10^1$	$4.44 \cdot 10^3$	$4.49 \cdot 10^3$	$4.49 \cdot 10^3$
	0.10	0.02	$1.85 \cdot 10^0$	$2.73 \cdot 10^1$	$2.92 \cdot 10^1$	$2.92 \cdot 10^1$
		0.15	$5.67 \cdot 10^0$	$9.30 \cdot 10^1$	$9.87 \cdot 10^1$	$9.87 \cdot 10^1$
		0.45	$4.99 \cdot 10^1$	$8.23 \cdot 10^2$	$8.73 \cdot 10^2$	$8.73 \cdot 10^2$

TABLE 1. Channel slip velocity values predicted by model $u^{mod} = \tilde{u}^{mod}/U^d$. Darcy contribution u_K^{mod} and Navier slip contribution u_L^{mod} are listed separately. Final column tabulates DNS result $u^{DNS} = \tilde{u}^{DNS}/U^d$.

problem in section 2, we revert to dimensional quantities,

$$u_i = - \left(\mathcal{K}_{ij} \frac{l^2}{\mu} \right) \tilde{p}_{,j} + \left(\mathcal{L}_{ijk} \frac{l}{\mu} \right) \Sigma_{jk}^u \quad \text{at} \quad \Gamma. \quad (3.12)$$

The coefficients based on solutions of the interface cell problems for the cavity flow are then $K_{cyl} = l^2 \mathcal{K}_{22}$, $K_s = l^2 \mathcal{K}_{11}$ and $L_s = l \mathcal{L}_{112}$. Since we are imposing $p = \tilde{p}$ along the interface, it is safe to set $\partial_x p = \partial_x \tilde{p}$ for this particular geometry, as reflected by no “tilde” above pressure in equation (2.2). For a general anisotropic bed, the condition on the pressure across the interface would also need to be determined, similar as done by Carraro *et al.* (2013). The pressure condition is out of scope of the current paper.

3.4. Accuracy of slip prediction and robustness to interface location

In order to illustrate more quantitatively that the proposed boundary condition yields accurate and robust slip velocity predictions, we turn our attention to the channel flow. We proceed in the same way as in section 2 by comparing the slip velocity predictions between DNS and continuum model. We also assess the contributions from two different terms in the derived boundary condition (3.12). Tab. 1 shows that for the range of parameters considered, the contribution at the interface from the Navier-slip term is always at least an order of magnitude larger than the contribution from the Darcy term. This is a consequence of (3.12), where $K \sim l^2$ and $L \sim l$, and therefore $K \ll L$ for fine micro-structures. For the channel flow, where the viscous forces are balanced by the pressure forces, one may therefore obtain a good approximation with only the Navier-slip term, as first suggested by Saffman (1971) and later rigorously shown by Mikelić & Jäger (2000). Including the Darcy term however yields – consistently – a much smaller error, and therefore also a *robust* velocity boundary condition with respect to the interface location and different pore geometries. Moreover, the Darcy term can be important if the pressure gradients are large, such as flows around bluff bodies.

4. Conclusions

Using multi-scale expansion, a general tensorial interface boundary condition has been derived with no free parameters. In contrast to the BJ condition, the proposed condition depends on the *interface* permeability and on the total stress. In order to determine the tensorial coefficients in the boundary condition, a group of microscale interface problems has to be solved. To the authors' knowledge, such a general formulation has not been presented and validated before. The present boundary condition has been used in effective models of both one and two dimensional flows and found to give robust slip velocity predictions for a range of volume fractions, scale separation parameters and interface locations. To make this work accessible, solvers for the microscale problems and the lid-driven cavity have been released as an open-source software (Lācis & Bagheri 2016).

REFERENCES

ABDULBARI, H.A., YUNUS, R.M., ABDURAHMAN, N.H. & CHARLES, A. 2013 Going against the flow-a review of non-additive means of drag reduction. *J. Ind. Eng. Chem.* **19** (1), 27–36.

AURIAULT, J.L. 2010 About the Beavers and Joseph boundary condition. *Transport Porous Med.* **83** (2), 257–266.

BEAVERS, G. S. & JOSEPH, D. D. 1967 Boundary conditions at a naturally permeable wall. *J. Fluid Mech.* **30** (01), 197–207.

CARRARO, T., GOLL, C., MARCINIAK-CZUCHRA, A. & MIKELIĆ, A. 2013 Pressure jump interface law for the stokes–darcy coupling: Confirmation by direct numerical simulations. *J. Fluid Mech.* **732**, 510–536.

DAVIT, Y., BELL, C.G., BYRNE, H.M., CHAPMAN, L.A.C., KIMPTON, L.S., LANG, G.E., LEONARD, K.H.L., OLIVER, J.M., PEARSON, N.C., SHIPLEY, R.J. *et al.* 2013 Homogenization via formal multiscale asymptotics and volume averaging: How do the two techniques compare? *Adv. Water Resour.* **62**, 178–206.

HAN, Y., GANATOS, P. & WEINBAUM, S. 2005 Transmission of steady and oscillatory fluid shear stress across epithelial and endothelial surface structures. *Phys. Fluids* **17** (3).

HECHT, F. 2012 New development in FreeFem++. *J. Numer. Math.* **20** (3-4), 251–265.

JONES, I.P. 1973 Low reynolds number flow past a porous spherical shell. In *Math. Proc. Cambridge*, , vol. 73, pp. 231–238. Cambridge Univ Press.

LĀCIS, U. & BAGHERI, S. 2016 <https://github.com/UgisL/MSEbc>.

LE BARS, M. & WORSTER, M. G. 2006 Interfacial conditions between a pure fluid and a porous medium: implications for binary alloy solidification. *J. Fluid Mech.* **550**, 149–173.

LIU, K. & JIANG, L. 2011 Bio-inspired design of multiscale structures for function integration. *Nano Today* **6** (2), 155–175.

MEI, C.C. & VERNESCU, B. 2010 *Homogenization methods for multiscale mechanics*. World scientific.

MIKELIĆ, A. & JÄGER, W. 2000 On the interface boundary condition of Beavers, Joseph, and Saffman. *SIAM J. Appl. Math.* **60** (4), 1111–1127.

MINALE, M. 2014 Momentum transfer within a porous medium. II. Stress boundary condition. *Phys. Fluids* **26** (12).

NIELD, D.A. 2009 The Beavers–Joseph boundary condition and related matters: a historical and critical note. *Transport Porous Med.* **78** (3), 537–540.

OCHOA-TAPIA, J.A. & WHITAKER, S. 1995 Momentum transfer at the boundary between a porous medium and a homogeneous fluid–I. Theoretical development. *Int. J. Heat and Mass Transfer* **38** (14), 2635 – 2646.

ROSTI, M.E., CORTELEZZI, L. & QUADRIDIO, M. 2015 Direct numerical simulation of turbulent channel flow over porous walls. *J. Fluid Mech.* **784**, 396–442.

SAFFMAN, P.G. 1971 On the boundary condition at the surface of a porous medium. *Stud. Appl. Math.* **50** (2), 93–101.

ZAMPOGNA, G. A. & BOTTARO, A. 2016 Fluid flow over and through a regular bundle of rigid fibres. *J. Fluid Mech.* **792**, 5–35.